This is a Just Accepted version, keep updated with https://doi.org/10.26599/EMD.2026.9370111
Energy Materials and Devices **2026, 4(4), 9370111**

Graphical Abstract

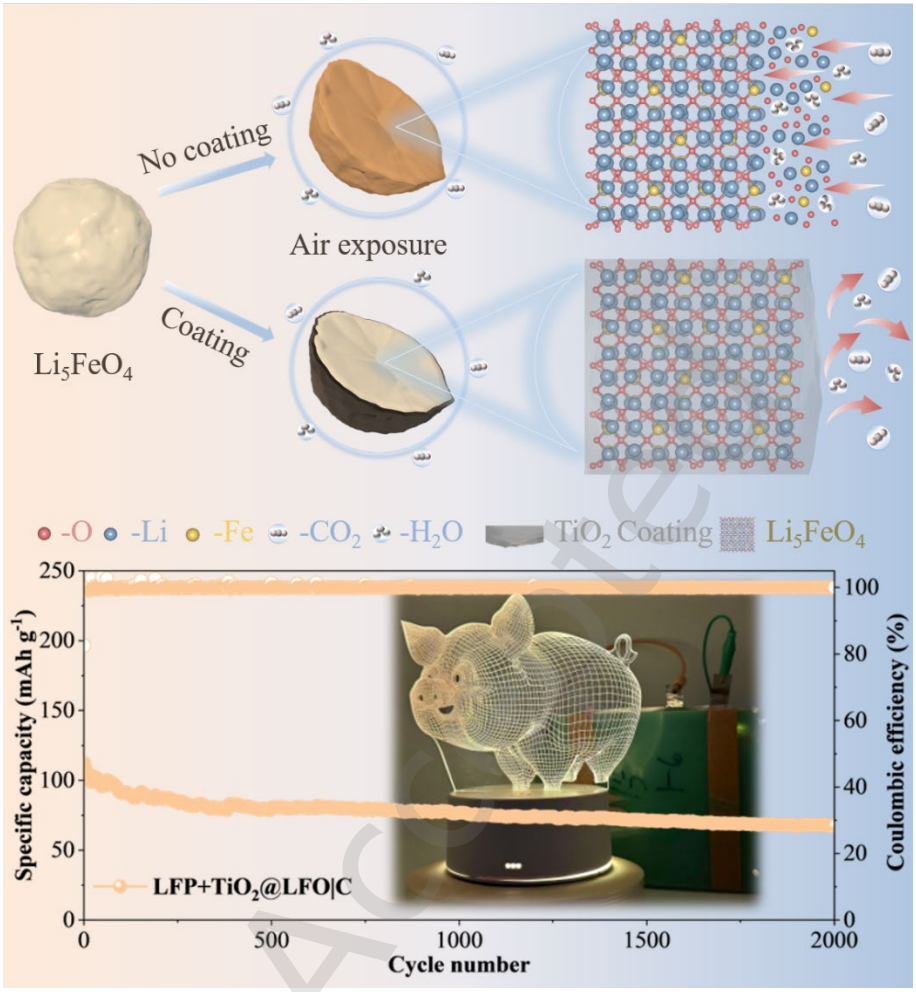

A TiO_2 coating strategy is developed to improve the air stability of Li_5FeO_4 prelithiation additives. The protective layer suppresses surface reactions with atmospheric H_2O and CO_2 while preserving effective lithium release. $LiFePO_4$/graphite pouch cells incorporating the coated additive demonstrate sustained cycling for 2,000 cycles, highlighting its potential for practical lithium compensation.

This is a Just Accepted version, keep updated with https://doi.org/10.26599/EMD.2026.9370111
Energy Materials and Devices **2026, 4(4), 9370111**

Research Article

Interfacial engineering enables air-stable Li_5FeO_4 prelithiation additives for long-Life $LiFePO_4$|graphite batteries

Ruijin He[a, b†], Bo Zhu[c,†], Zhenyu Jiang[c,*], Ming Ma[a, b], Minying Wu[a, b], Qiang Fu[a, b], Zhengrong Liu[a, b*], Qing Li[c,*]

[a]*Electric Power Research Institute, Guangdong Power Grid Co., Ltd., Guangzhou 510080, China*
[b]*China Southern Power Grid Laboratory for New Energy Grid Integration and Accommodation, Guangzhou 510080, China*
[c]*Macao Centre for Research and Development in Advanced Materials, Institute of Applied Physics and Materials Engineering, University of Macau, Macao 999078, China*

*Address correspondence to yc57840@um.edu.mo (Z. Jiang), liu0zheng0rong@163.com (Z. Liu), liqing@um.edu.mo (Q. Li)

Received: July 15, 2026 / **Revised:** August 17, 2026 / **Accepted:** September 2, 2026

Abstract

Lithium iron phosphate ($LiFePO_4$, LFP)|graphite (Gr) full cells are widely used in large-scale energy storage owing to their safety and long cycling stability. However, irreversible lithium consumption during solid electrolyte interphase (SEI) formation depletes the limited lithium inventory, causing initial capacity loss and compromising the cycling stability of full cells. Lithium-rich lithium ferrite (Li_5FeO_4, LFO) has emerged as a promising cathode prelithiation additive for compensating lithium loss, but its poor air stability and moisture sensitivity restrict practical application. Herein, we introduce a TiO_2 interfacial coating strategy to stabilize LFO by constructing a nanoscale protective layer on particle surfaces. The TiO_2 coating preserves the antifluorite structure of LFO while suppressing surface degradation and improving electrode processing compatibility. The optimized 1.5% TiO_2@LFO maintains structural integrity after air exposure for 2 h and effectively mitigates slurry gelation. In LFP|Gr full cells, TiO_2@LFO delivers an irreversible delithiation plateau at 3.5–4.0 V, compensating for SEI-related lithium consumption and increasing the initial

discharge capacity from 160 to 175 mAh g^{-1}. Moreover, TiO_2@LFO enables stable cycling over 500 cycles at 1C, while LFP|Gr pouch cells achieve 60% capacity retention after 2000 cycles and remain capable of powering an LED lamp. This work provides an effective interfacial engineering approach for developing air-stable LFO prelithiation additives toward practical high-energy-density lithium-ion batteries.

Keywords: long cycling stability; cathode prelithiation additive; Li_5FeO_4; surface coating; TiO_2

1. Introduction

With the rapid development of renewable energy and electrification technologies, advanced electrochemical energy storage systems with high safety, long lifespan, and reliable performance are increasingly demanded[1–4]. Among various battery technologies, lithium iron phosphate ($LiFePO_4$, LFP)|graphite (Gr) full cells have attracted extensive attention for large-scale energy storage applications owing to their excellent thermal stability, low cost, and outstanding cycling durability[5–8]. However, during the initial charging stage, the electrolyte undergoes reductive decomposition on the surface of graphite anodes to form a solid electrolyte interface (SEI) film. This irreversible process consumes approximately 5%–10% of the active lithium within the cell[9–11]. For LFP systems, which possess a theoretical specific capacity of 170 mAh g^{-1}, this irreversible lithium loss directly reduces the initial available capacity and decreases the lithium utilization efficiency of full cells. As cycling progresses, there is a continuous consumption of active lithium due to persistent interfacial side reactions and SEI film evolution. This, in turn, accelerates capacity fading and deteriorates the cycling stability of batteries, as well as the service life of energy storage systems[12,13]. Consequently, the implementation of cathode lithium compensation strategies to offset initial lithium loss is of great significance for enhancing capacity utilization, cycling stability and the economic performance of LFP energy storage batteries.

To compensate for the initial cycle lithium loss, introducing sacrificial lithium supplement additive on the cathode side is regarded as an engineeringly feasible strategy[14,15]. Among various candidates, Li_5FeO_4 (LFO) has attracted considerable

research interest owing to its anti-fluorite crystal structure and ultrahigh lithium content. Within its crystal framework, oxygen atoms form a face-centered cubic skeleton, while Li^+ and Fe^{3+} jointly occupy tetrahedral interstitial sites. Benefiting from its lithium-rich characteristic, LFO can deliver a lithium source with a specific capacity exceeding 700 mAh g^{-1} during the initial charging process[16]. In addition, both LFO and LFP belong to iron-based material systems, and no transition metal ions such as Ni or Co are introduced in its reaction products, which helps to prevent disruption to the SEI film structure on the anode[17]. Nevertheless, significant challenges persist in the practical application of LFO. LFO is highly sensitive to H_2O and CO_2 in ambient air, readily generating insulating byproducts including LiOH and Li_2CO_3 on its surface. These impurities not only degrade the intrinsic electrochemical activity of the material but also trigger severe gelation during electrode slurry preparation[18,19]. Meanwhile, the delithiated residual phase of LFO exhibits low electronic conductivity, thereby further constraining the electrode reaction kinetics[20]. In recent years, researchers have attempted multiple modification approaches to address the poor environmental stability of LFO, such as carbon coating, inorganic salt modification and interfacial structure regulation[21–24]. For instance, the application of carbon coating has been demonstrated to enhance the electronic conductivity and mitigate air corrosion of LFO, yet it offers limited barrier performance against moisture and CO_2. Although certain inorganic coatings can improve surface stability, their interfacial compatibility and structural integrity under high potential conditions still require further optimization. Consequently, the development of a coating strategy that simultaneously achieves superior environmental stability, interfacial chemical inertness and structural robustness is imperative to advance the practical deployment of LFO as a lithium supplement additive.

As illustrated in Fig. 1, titanium dioxide (TiO_2) with superior chemical stability was selected as the interfacial coating material in this work. Building on previous research into surface coatings and interfacial regulation[25–28], a TiO_2 protective layer was formed on the surface of LFO particles through the controlled hydrolysis of tetrabutyl titanate. This coating layer acts as a physical barrier, suppressing the

corrosion of LFO by H_2O and CO_2 in ambient air. Meanwhile, TiO_2 possesses a high lithium intercalation potential and favorable interfacial stability, which mitigates side reactions under high-voltage conditions[29,30]. From the perspective of interfacial structure engineering, this work systematically investigates the effects of TiO_2 coating content on the crystal structure, surface chemistry, air stability, and slurry processing compatibility of LFO. Combined with electrochemical tests of coin full cells and pouch full cells, the lithium compensation performance and cycling stability of TiO_2@LFO are comprehensively verified. The obtained results provide experimental support for improving the environmental adaptability and practical application feasibility of the LFO sacrificial lithium additive.

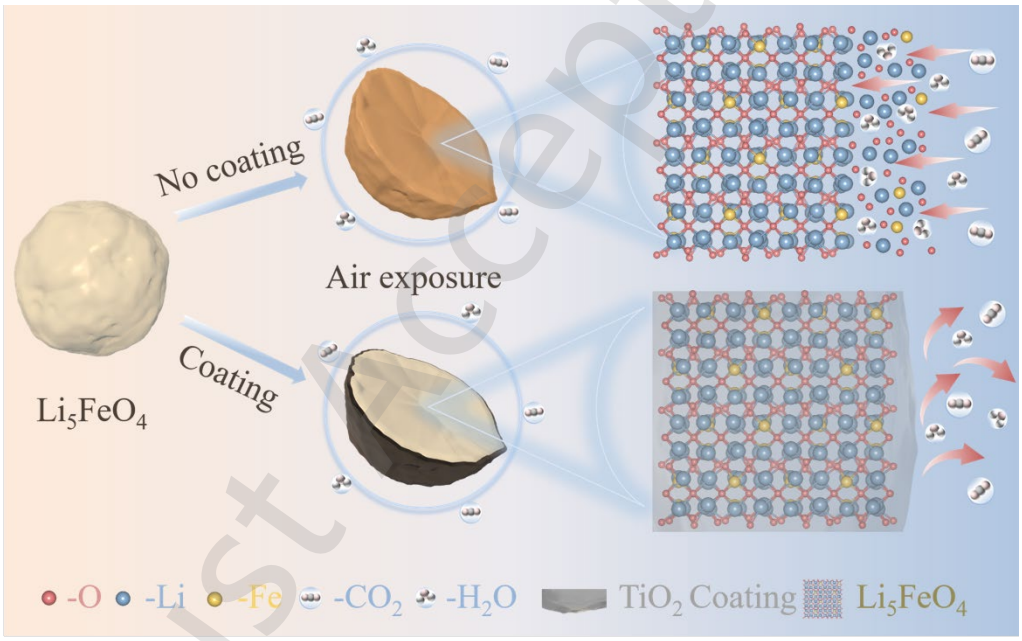

Fig. 1. Schematic illustration of the preparation process of TiO_2@LFO.

2. Experimental section

2.1. Materials

Lithium oxide (Li_2O, 99.9% purity), ferric oxide (Fe_2O_3), tetrabutyl titanate (TBOT) and anhydrous ethanol were purchased from Aladdin. Lithium iron phosphate (LFP), artificial graphite, polyvinylidene fluoride (PVDF), and conductive carbon black (Super P) were purchased from Guangdong Canrud New Energy Technology Co.,Ltd.. All chemical reagents employed in this work were of analytical grade and were used without further purification. The conventional energy-storage electrolyte consists of 1

mol L^{-1} $LiPF_6$ dissolved in a mixed solvent of EC:DMC:EMC with a volume ratio of 1:1:1.

2.2. Preparation of lithium additives

The LFO precursor was synthesized via a high-temperature solid-state reaction method. Given the severe volatilization of lithium sources during high-temperature calcination, precise weighing was performed at a molar ratio of Li_2O:Fe_2O_3 = 5.2:1 (4% excess lithium source) for raw material preparation. The mixed powders were transferred into a milling jar and ball-milled for 10 h to achieve homogeneous mixing of reactants. Afterwards, the powder mixture was placed in a tube furnace and calcined at a constant temperature of 750 °C for 20 h under an argon protective atmosphere. After natural furnace cooling to room temperature, the product was collected, ground and sieved inside a glovebox to obtain Li_5FeO_4 active powder with an anti-fluorite structure.

Specifically, inside a glovebox, TBOT was dissolved in anhydrous ethanol under ultrasonic dispersion, followed by the addition of LFO powder, synthesized via the aforementioned procedure, with continuous magnetic stirring. TBOT gradually underwent hydrolysis by absorbing trace water inside the system, in situ forming a TiO_2 gel coating layer on the surface of LFO particles. The solvent of the suspension was evaporated under vacuum at 80 °C to obtain precursor powders. The precursors were transferred to a tube furnace and heat-treated at 450 °C for 4 h under an argon atmosphere. After cooling and grinding, TiO_2@LFO sacrificial lithium supplement additives with TiO_2 mass fractions of 1.0%, 1.5% and 2.0% were successfully prepared.

2.3. Characterization methods

The crystal structure and phase composition of the samples were characterized by X-ray diffraction (XRD) with the range of 10°–80° (2θ). Raman spectroscopy was utilized to analyze the structural features and surface components of the materials. Scanning electron microscopy (SEM) was adopted to observe the micromorphology of samples, and energy dispersive spectroscopy (EDS) was coupled to analyze elemental distribution. Transmission electron microscopy (TEM) was further employed to characterize the microstructure of particles and the morphology of the surface coating

layer. X-ray photoelectron spectroscopy (XPS) was used to investigate the surface elemental composition and chemical valence states of the materials.

To evaluate the environmental stability of the materials, all powder samples were exposed to ambient air with a relative humidity of approximately 30% for 2 h. Subsequent XRD measurements were carried out to analyze the resulting phase evolution, and SEM together with TEM were applied to observe morphological variations. Meanwhile, the exposed powders were mixed with conductive agent and polyvinylidene fluoride (PVDF) to prepare electrode slurries. The processing compatibility of the materials during electrode fabrication was evaluated by observing the macroscopic morphology and fluidity variations of slurries, including gelation and agglomeration behaviors.

2.4. Electrochemical performance testing

To investigate the effects of TiO_2 coating on the delithiation behavior and interfacial reaction kinetics of LFO, CR2032 coin-type half-cells were first assembled for electrochemical measurements. Coin half-cells were mainly adopted to analyze the initial charge-discharge profiles, cyclic voltammetry responses, and electrochemical impedance evolution of the materials, providing experimental evidence for the lithium compensation mechanism analysis. All coin cells were assembled in an argon-filled glovebox. The working electrode was fabricated by mixing active LFO material, conductive carbon black (Super P) and polyvinylidene fluoride (PVDF) binder at a mass ratio of 90:5:5, followed by coating the slurry onto an aluminum foil current collector. Lithium metal foil served as the counter electrode, Celgard 2400 was used as the separator, and the electrolyte was 1 mol L^{-1} $LiPF_6$ dissolved in a mixed solvent of EC, DMC and EMC with a volume ratio of 1:1:1. Galvanostatic charge-discharge, cyclic voltammetry (CV) and electrochemical impedance spectroscopy (EIS) tests were performed on LFO|Li half-cells within a voltage window of 2.5–4.3 V. The CV scan rate was set to 0.05 mV s^{-1}, and the frequency range for EIS measurements spanned from 10^5 to 10^{-2} Hz.

LFP|Li half-cells were further assembled to evaluate the influence of lithium supplement additives on the electrochemical performance of LFP electrodes. The

working electrode was composed of LFP, Super P, and PVDF at a mass ratio of 90:5:5. For the experimental groups, an extra 3 wt% lithium supplement additive (relative to the mass of LFP) was incorporated, while the proportions of other components remained unchanged. Lithium metal foil was used as the counter electrode, and all other assembly parameters were identical to those of the aforementioned LFO|Li half-cells. Moreover, LFP|graphite full cells were constructed to verify the practical lithium compensation performance of the supplement additive in realistic battery systems. The cathode formulation was consistent with that of the LFP half-cells, and graphite was employed as the anode. Galvanostatic charge-discharge and long-cycle tests were conducted on full cells at a voltage range of 2.5–4.2 V, and their rate capability was evaluated simultaneously. To further confirm the practical viability of TiO_2@LFO in pouch cell systems, lab-scale pouch full cells were assembled using TiO_2@LFO-modified LFP cathodes and graphite anodes. Galvanostatic charge-discharge and cycling measurements were carried out within a voltage window of 2.5–3.65 V. These tests were designed to assess the electrochemical adaptability of the lithium supplement additive during electrode slurry preparation, pouch cell assembly, and long-term cycling operation.

3. Results and discussion

3.1. Structural and morphological analysis

The crystal structure and surface chemical composition of the materials were characterized by XRD and Raman spectroscopy. As shown in Fig. 2a, the diffraction peaks of the pristine LFO are in close agreement with the standard anti-fluorite structure of Li_5FeO_4 (PDF#00-024-0623), with no detectable impurity phases, indicating that a phase-pure product was successfully obtained via solid-state synthesis. Following the TiO_2 coating process (Fig. 2b), the diffraction patterns of samples with varying coating amounts (1.0%, 1.5%, and 2.0%) remain essentially consistent with those of the pristine LFO, and no discernible diffraction peaks attributable to TiO_2 are observed, suggesting that the coating process does not significantly affect the host crystal structure of LFO. Given the relatively low coating content and the possible presence of TiO_2 in an

amorphous or nanocrystalline form, the corresponding diffraction signals may fall below the detection limit of XRD. It is worth noting that within the investigated coating range of 1.0%–2.0%, even the 2.0% TiO_2@LFO sample does not exhibit any distinct crystalline TiO_2 diffraction peaks, indicating that TiO_2 predominantly exists on the particle surface in a low-crystallinity or nanodispersed state within this compositional window. To further elucidate the chemical nature and presence of the surface coating layer, Raman spectroscopy was performed on the samples. As illustrated in Fig. 2c, the pristine LFO displays characteristic lattice vibration peaks in the low-wavenumber region. In comparison, TiO_2@LFO retains the characteristic Raman bands of LFO. Crystalline anatase TiO_2 typically exhibits Raman modes at approximately 144, 197, 399, 513/519, and 639 cm^{-1}, whereas rutile TiO_2 shows characteristic bands at approximately 143, 447, and 612 cm^{-1}. However, no well-resolved diagnostic bands corresponding to either phase are observed for TiO_2@LFO, precluding an unambiguous assignment to crystalline anatase or rutile. Together with the absence of detectable TiO_2 reflections in the XRD patterns, these results suggest that the in situ formed coating is predominantly amorphous or poorly crystallized. The surface presence of TiO_2 is instead confirmed by the Ti 2p XPS signal and TEM observations (Figure 3b, e, f). The structurally disordered TiO_2 layer may provide defect-mediated and relatively isotropic Li^+ transport pathways while protecting the reactive LFO surface; however, an excessively thick coating would increase the Li^+ migration distance and interfacial resistance. Therefore, optimizing the coating content is essential to balance surface protection and Li^+transport kinetics. The present study focuses on elucidating the modulatory effects of TiO_2 within the low-coating range of 1.0%–2.0% on the air stability, slurry processability, and lithium compensation performance of LFO. In addition, weak D and G bands are observed in the high-wavenumber region, which are typically associated with disordered and graphitic carbon species, respectively. These signals are likely attributable to residual carbon formed by the incomplete decomposition and in situ carbonization of tetrabutyl titanate during the heat-treatment process. It should be noted that the residual carbon content is relatively low and exerts only a limited influence on the host crystal structure. Nevertheless, the coexistence of

residual carbon with TiO_2 has been shown to moderately improve the interfacial contact state, thereby exerting a positive effect on subsequent electrochemical reactions.

From a morphological standpoint, as shown in Fig. 2d, the pristine LFO particles exhibit a relatively rough surface with well-defined boundaries. Following the TiO_2 coating process (Fig. 2e–f), taking 1.5% TiO_2@LFO as a representative, the particle surface is observed to be covered by a continuous phase, with the overall morphology tending to become smoother and denser. To further verify the distribution of the coating layer, EDS elemental mapping was conducted on this sample. As illustrated in Fig. 2g, O, Fe, and Ti elements are uniformly distributed across the particle domains, with no evident elemental segregation, indicating that Ti species have achieved relatively homogeneous coverage on the particle surface. The structural and morphological results confirm that a uniformly distributed TiO_2 coating layer has been successfully constructed on the LFO particle surface via a liquid-phase hydrolysis process. This tailored architecture, while preserving the pristine bulk crystal structure, provides a foundational basis for the subsequent regulation of interfacial stability.

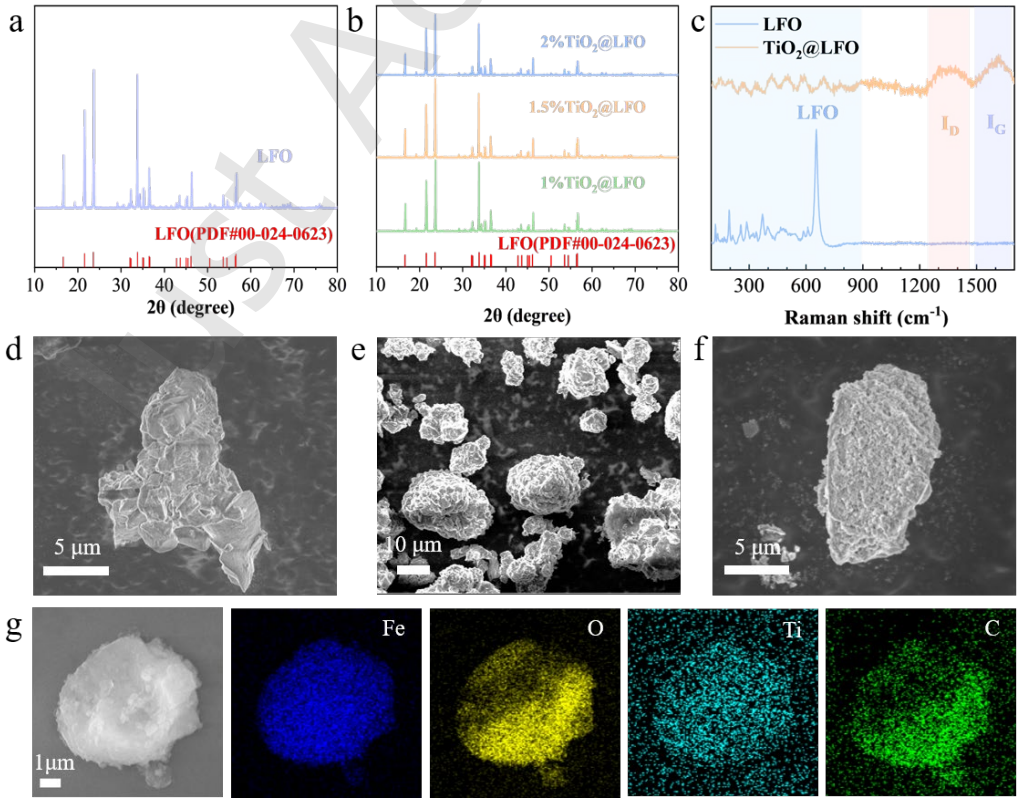

Fig. 2. a XRD pattern of pristine LFO; b XRD patterns of LFO with different TiO_2 coating

contents; c Raman spectra of pristine LFO and TiO_2-coated LFO; d SEM image of pristine LFO; e, f SEM images of 1.5% TiO_2@LFO; g EDS elemental mapping of 1.5% TiO_2@LFO.

3.2. Chemical structure analysis

To further elucidate the surface chemical composition and the structural characteristics of the coating layer, XPS was conducted on both pristine LFO and TiO_2@LFO samples. The survey spectra (Supplementary Fig. 1a) reveal that the surface of pristine LFO is primarily composed of Fe, O, C, and Li elements. Upon TiO_2 coating, a distinct Ti 2p signal emerges, accompanied by a marked attenuation of the Fe-related signals, indicating a substantial alteration of the surface chemical environment. The high-resolution Fe 2p spectra are presented in Fig. 3a. The pristine LFO exhibits two characteristic peaks at approximately 710.5 eV and 724.0 eV, corresponding to Fe $2p_{3/2}$ and Fe $2p_{1/2}$, respectively, along with typical satellite features, confirming that iron exists primarily in the form of Fe^{3+}, which is consistent with the structural configuration of Li_5FeO_4. Conversely, for the TiO_2@LFO sample, the Fe 2p signal is significantly attenuated, approaching the detection limit and leaving only a weak background response. Given that the effective probing depth of XPS is generally in the range of 5–10 nm, this pronounced signal suppression strongly suggests that a relatively continuous TiO_2 overlayer has been formed on the particle surface, effectively screening the substrate signal. Figure 3b displays the high-resolution Ti 2p spectrum of the TiO_2@LFO sample, where the Ti $2p_{3/2}$ and Ti $2p_{1/2}$ peaks are located at 458.5 eV and 464.3 eV, respectively, with a spin–orbit splitting of approximately 5.8 eV. These values are characteristic of Ti^{4+}, and the absence of discernible low-valence Ti species indicates that the TiO_2 structure remains stable during the calcination process. Furthermore, as shown in Supplementary Fig. 1b, the Li 1s signal of the TiO_2@LFO sample is notably weaker than that of pristine LFO. This attenuation can be reasonably attributed to the enhanced inelastic scattering and signal damping effects induced by the surface coating layer, which suppress the photoemission from the underlying LFO matrix. The O 1s high-resolution spectra (Fig. 3c) further reveal the evolution of surface chemical states. For pristine LFO, the O 1s spectrum consists of multiple overlapping components, with the higher-binding-energy region (~531.5 eV and ~533.0 eV)

primarily corresponding to C=O and C–O bonds from surface carbonate/organic residues, whereas the lattice oxygen signal at the lower-binding-energy side appears relatively weak. This observation suggests that the pristine LFO surface is likely covered by a layer of carbonate or organic contaminants, which masks the intrinsic lattice oxygen signal. In contrast, the TiO_2@LFO sample exhibited a prominent low-binding-energy peak at around 529.0 eV, attributable to the lattice oxygen of Ti–O bonds. This peak became the predominant component, indicating that TiO_2 now exerts a dominant influence on the surface chemical environment. In addition, the C 1s spectrum (Fig. 3d) reveals minor C–C, C–O, and O–C=O components, which may originate from precursor decomposition residues or carbonate species formed upon exposure to air. The relatively weak intensity of these signals suggests a limited amount of surface carbonaceous species. The formation and morphology of the protective layer were further examined by TEM. The pristine LFO particle shows a relatively rough surface without a clearly distinguishable coating layer (Fig. 3e). In comparison, TiO_2@LFO exhibits a continuous interfacial layer surrounding the LFO particle (Fig. 3f). The thickness of this TiO_2-rich layer is approximately 130 nm, as indicated by the dashed boundaries. These XPS and TEM results collectively confirm the successful construction of a continuous TiO_2 coating on the LFO surface. The coating effectively isolates the reactive LFO core from direct exposure to the external environment and is therefore expected to suppress surface degradation and improve the air stability of LFO.

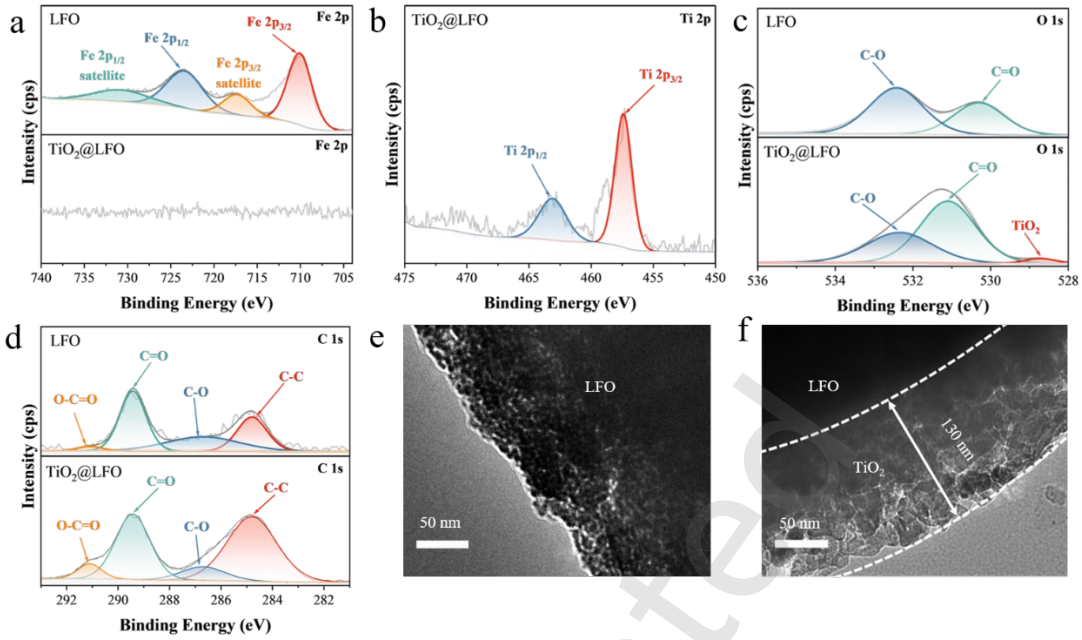

Fig. 3. High-resolution XPS spectra and TEM characterization of LFO and TiO_2@LFO: a Fe 2p spectra of pristine LFO (top) and TiO_2@LFO (bottom); b Ti 2p spectrum of TiO_2@LFO; c O 1s spectra of pristine LFO (top) and TiO_2@LFO (bottom); d C 1s spectra of pristine LFO (top) and TiO_2@LFO (bottom); e TEM image of pristine LFO; and f cross-sectional TEM image of TiO_2@LFO showing a TiO_2-rich layer with a representative thickness of approximately 130 nm.

3.3. Air stability analysis

A major challenge limiting the practical application of LFO as a prelithiation additive is its high sensitivity to ambient moisture and carbon dioxide. The highly reactive lithium species at the LFO surface can readily interact with H_2O and CO_2, resulting in surface reconstruction and the formation of undesirable lithium-containing by-products. These surface reactions not only deteriorate the structural integrity of LFO but also impair its compatibility with electrode processing. To investigate the protective effect of TiO_2 coating, pristine LFO and TiO_2@LFO samples were exposed to air with a relative humidity of 30% for 2 h, followed by structural and processability evaluations. As shown in Fig. 4a, pristine LFO exhibits an obvious color change from light yellow to brownish orange after air exposure, indicating severe surface degradation. In contrast, TiO_2@LFO maintains its original appearance, suggesting enhanced environmental stability. XRD analysis further confirms the distinct degradation behaviors of the two samples (Fig. 4b). After exposure, LFO presents additional diffraction peaks

corresponding to LiOH, Li_2CO_3, and $LiFeO_2$, demonstrating the occurrence of surface chemical transformation. These products originate from the reaction between surface lithium species and atmospheric H_2O/CO_2, accompanied by partial lattice reconstruction. In comparison, TiO_2@LFO retains the characteristic diffraction peaks of the LFO phase without detectable impurity phases, indicating that the TiO_2 coating effectively suppresses surface reactions and preserves the structural integrity of LFO. The microscopic evolution of LFO after air exposure is further revealed by TEM observations. As shown in Fig. 4c, severe surface corrosion and abundant amorphous/secondary phases are observed on exposed LFO particles, accompanied by unclear particle boundaries and disrupted surface morphology. In contrast, TiO_2@LFO particles maintain well-defined contours(Fig. 4d), with no obvious by-product deposition, further demonstrating the protective capability of the TiO_2 interfacial layer.

The formation of lithium-containing surface species also significantly affects slurry processing. During electrode fabrication, the alkaline $LiOH/Li_2CO_3$ species generated on degraded LFO surfaces can interact with PVDF binders, causing dehydrofluorination and promoting undesirable crosslinking reactions[31,32]. As a result, the LFO-based slurry exhibits severe gelation and poor fluidity (Fig. 4e). By suppressing the formation of reactive surface species, the TiO_2 coating prevents detrimental interactions between LFO and the binder system. Consequently, the TiO_2@LFO slurry maintains good dispersion and fluidity, enabling improved electrode processing compatibility (Fig. 4f). The enhanced air stability of TiO_2@LFO can be attributed to the conformal TiO_2 coating, which acts as an effective interfacial barrier against external H_2O/CO_2 penetration while regulating surface lithium reactivity. This interfacial stabilization strategy simultaneously inhibits surface degradation and preserves slurry processability, providing a practical approach for improving the environmental tolerance of LFO prelithiation additives.

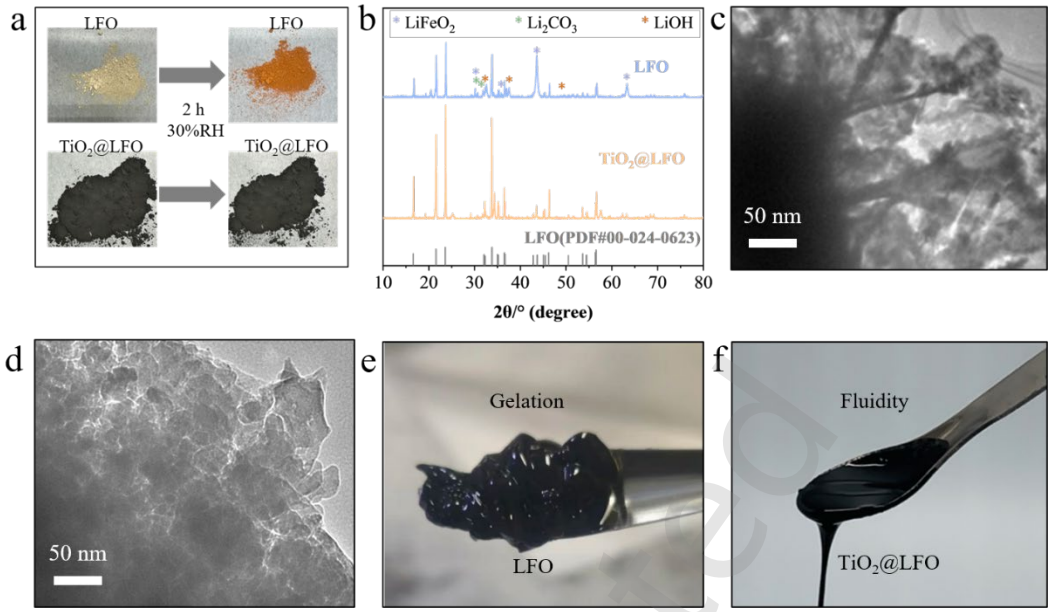

Fig. 4. a Optical images of LFO and TiO_2@LFO powder after exposure; b XRD patterns after air exposure for 2 h; c, d TEM image of (c)LFO and (d)TiO_2@LFO after exposure; e, f Slurry state of e LFO and f TiO_2@LFO after exposure.

3.4. Battery performance analysis

To further evaluate the influence of TiO_2 coating on the interfacial reaction kinetics and lithium compensation behavior of the materials, a series of systematic electrochemical characterizations were performed. Figure 5a presents the initial charge–discharge curves of samples with varying coating amounts, with the corresponding parameters summarized in Supplementary Table S1. Pristine LFO delivers a first-charge delithiation capacity of 575 mAh g^{-1}, with its main lithium-release plateau located at 3.6–4.3 V and accompanied by pronounced charging polarization. After TiO_2 modification, the first-charge delithiation capacities increase to 704 and 720 mAh g^{-1} for 1.0% TiO_2@LFO and 1.5% TiO_2@LFO, respectively, while the main lithium-release plateau shifts to a lower voltage range of 3.5–4.3 V. These results indicate that an appropriate TiO_2 coating alleviates interfacial polarization and promotes the extraction of active lithium from LFO during the first charge, thereby improving its lithium-compensation capability. Among the coated samples, 1.5% TiO_2@LFO delivers the highest initial charge capacity; notably, its initial discharge capacity also increases from 21 mAh g^{-1} (for pristine LFO) to 71 mAh g^{-1}, indicating

concurrent improvements in both electrode reaction kinetics and interfacial stability at this optimal coating level. In contrast, further increasing the TiO_2 content from 1.5% to 2.0% leads to a pronounced deterioration in electrochemical performance. The first-charge capacity decreases from 720 to 619 mAh g^{-1}, accompanied by a sharp decline in the first-discharge capacity from 71 to 23 mAh g^{-1}. Because the first-charge capacity primarily reflects the amount of Li that can be extracted from LFO, the simultaneous decrease in both charge and discharge capacities suggests a loss of electrochemically accessible LFO rather than enhanced irreversible lithium compensation. This deterioration is likely associated with excessive TiO_2 coverage, which may form a thicker and locally aggregated surface layer and thereby increase the effective Li^+ transport distance to the underlying LFO. At the same time, excessive surface coverage can reduce electrolyte accessibility and partially block electrochemically active sites, resulting in increased interfacial charge-transfer resistance. These coupled transport and interfacial limitations suppress both Li^+ extraction during charging and subsequent Li^+ reinsertion during discharge, ultimately limiting the accessible capacity. Thus, beyond the optimal TiO_2 loading, the additional protective benefit of the coating is outweighed by the associated penalties in Li^+ transport and interfacial kinetics, leading to the observed capacity loss at 2.0% TiO_2. Considering the combined metrics of initial charge capacity, discharge capacity, and delithiation voltage characteristics, 1.5% TiO_2@LFO is identified as the optimal formulation with superior lithium compensation performance in this study.

To gain further insight into the interfacial charge-transfer kinetics, electrochemical impedance spectroscopy (EIS) was performed on the LFO|Li and 1.5% TiO_2@LFO|Li half-cells before and after the first charge. The corresponding Nyquist plots and equivalent circuit are shown in Fig. 5b, and the fitted parameters are summarized in Supplementary Table S2. Before charging, the pristine LFO electrode exhibits series resistance (R_s) and charge-transfer resistance (R_{ct}) values of 2.116 Ω and 50.85 Ω, respectively. By comparison, the 1.5% TiO_2@LFO electrode exhibits R_s and R_{ct} values of 1.779 and 46.80 Ω, respectively. The comparable Rs values indicate that the TiO_2 coating does not introduce an appreciable ohmic penalty, whereas the lower R_{ct} suggests

a reduced interfacial charge-transfer barrier and facilitated Li^+ extraction during the first charge. After the first charge, the R_s values of LFO and 1.5% TiO_2@LFO remain comparable at 2.179 and 2.012 Ω, respectively, while their Rct values decrease markedly to 18.86 and 14.55 Ω. The pronounced decrease in R_{ct} indicates enhanced interfacial charge-transfer kinetics following irreversible Li^+ extraction and electrochemical activation during the first charge. Notably, 1.5% TiO_2@LFO consistently exhibits a lower R_{ct} than pristine LFO both before and after the first charge, confirming that the optimized coating preserves favorable interfacial charge-transfer kinetics without imposing an additional kinetic barrier. Combined with the structural and air-stability results, these findings demonstrate that an optimized TiO_2 coating balances surface protection with favorable interfacial kinetics, thereby facilitating active-lithium release and improving the lithium-compensation performance of LFO. To elucidate the lithium compensation behavior of the material in a full-cell configuration, differential capacity (dQ/dV) curves at low rates (Fig. 5c) and CV profiles (Fig. 5d) were analyzed. The pristine LFP exhibits typical and symmetric reversible redox peaks. Upon incorporation of 1.5% TiO_2@LFO, an additional broad peak emerges within the 3.6–4.2 V region during the charging process, corresponding to an anodic current response initiating at approximately 3.6 V in the forward CV scan. This feature is attributable to the irreversible delithiation reaction of LFO during the initial charge ($Li_5FeO_4 \rightarrow LiFeO_2 + 4Li^+ + 4e^-$, accompanied by structural rearrangement), which releases active lithium ions into the system. During the subsequent discharge, the reduction peak in this high-voltage region essentially disappears, leaving only the characteristic reduction peak of LFP at approximately 3.3 V, confirming the distinctly irreversible nature of this reaction.

Figure 5e further presents the voltage profiles during the initial charge–discharge process at 0.1C. The pristine LFP displays a typical flat charging plateau at approximately 3.4 V, delivering an initial charge specific capacity of about 160 mAh g^{-1}. In contrast, the LFP+TiO_2@LFO composite electrode exhibits an additional charging plateau in the 3.5–4.2 V range following the 3.4 V plateau, corresponding to the delithiation process of the lithium compensator. Compared with the pristine LFO,

which typically manifests a sudden voltage surge and pronounced polarization, the TiO_2@LFO composite displays a more gradual and continuous charging profile, indicating mitigated polarization during the activation process. This improvement can be attributed to the fact that the coating layer optimizes the interfacial contact to a certain extent and helps maintain interfacial stability at elevated potentials. Benefiting from the extra active lithium released by TiO_2@LFO during the initial charge, which partially compensates for the irreversible lithium loss incurred during the formation of the solid electrolyte interphase (SEI) on the anode, the initial Coulombic efficiency of the system is enhanced. Consequently, the initial discharge specific capacity of the composite electrode increases from approximately 160 mAh g^{-1} for pristine LFP to about 175 mAh g^{-1}.

To evaluate the kinetic performance, the 1.5% TiO_2@LFO was incorporated into the LFP cathode and assembled into full cells with graphite anodes for rate capability testing (Fig. 5f). At various C-rates ranging from 0.2C to 2C, the composite electrode consistently delivers higher discharge capacities than the pristine LFP counterpart. Moreover, when the current rate is restored to 0.2C, the capacity is essentially recovered, indicating favorable reversibility and structural stability of the system. These results demonstrate that the TiO_2 coating introduces the lithium compensation functionality without imposing any significant adverse effect on the rate capability of the electrode.

To assess the long-term cycling stability, the coin-type LFP|graphite full cells were cycled at 1C for 500 cycles within a voltage range of 2.5–4.2 V (Fig. 5g). During the initial cycling stage, the LFP+TiO_2@LFO|C cell delivers a discharge capacity of approximately 145 mAh g^{-1}, which is higher than that of the reference system without a lithium compensator (approximately 125 mAh g^{-1}). As cycling proceeds, the capacity of the reference cell gradually decays, whereas the composite electrode maintains a capacity above approximately 125 mAh g^{-1} after 500 cycles, with the Coulombic efficiency consistently approaching 100%. This result indicates that the TiO_2-coated LFO not only achieves effective lithium compensation during the first charge but also, through its coating architecture, potentially mitigates sustained side reactions between the delithiated residual phase and the electrolyte, thereby retarding interfacial

462 impedance growth and capacity fade. An optimal amount of TiO_2 coating realizes a
463 synergistic optimization of lithium compensation efficiency and cycling stability
464 without compromising the lithium compensation functionality of LFO. To further
465 evaluate the practical applicability of TiO_2@LFO, LFP|graphite pouch cells were
466 assembled and cycled at 1C within a voltage range of 2.5–3.65 V. As shown in Figure
467 5h, the pouch cell incorporating the LFP+TiO_2@LFO cathode delivers an initial
468 discharge specific capacity of 112 mAh g^{-1}, confirming that TiO_2@LFO effectively
469 functions as a lithium compensator during the formation process of pouch cells,
470 offsetting part of the active lithium consumed by SEI formation on the graphite anode.
471 After 2,000 cycles, the pouch cell retains 60% of its initial capacity, indicating that
472 TiO_2@LFO does not induce uncontrolled parasitic side reactions within the pouch cell
473 configuration and that the battery maintains sustained long-term operation. At the same
474 1C rate, the coin cell in Fig. 5g delivers an initial discharge capacity of approximately
475 145 mAh g^{-1}, compared with 112 mAh g^{-1} for the pouch cell. The lower pouch-cell
476 capacity is partly attributable to its narrower voltage window and may also reflect cell-
477 format-dependent differences in electrode loading, compaction density, electrolyte
478 availability, electrode wetting, stack pressure, and current-distribution uniformity.
479 Throughout the long-term cycling, the Coulombic efficiency of the pouch cell remains
480 at a consistently high level, suggesting that TiO_2@LFO primarily undergoes
481 irreversible delithiation and releases active lithium during the initial charge stage,
482 without continuously consuming electrolyte or triggering severe interfacial side
483 reactions in subsequent cycles. To visually demonstrate the actual energy output
484 capability of the pouch cell after prolonged cycling, an LED lamp was powered by the
485 LFP+TiO_2@LFO pouch cell. As shown in the inset of Fig. 5h, the pouch cell is capable
486 of steadily driving the LED lamp, demonstrating that it still retains effective electrical
487 energy output after extended cycling. Collectively, these results further substantiate that
488 the TiO_2@LFO lithium compensator not only exhibits favorable lithium compensation
489 performance in coin cells but also demonstrates viable application potential in pouch-
490 type full cells.

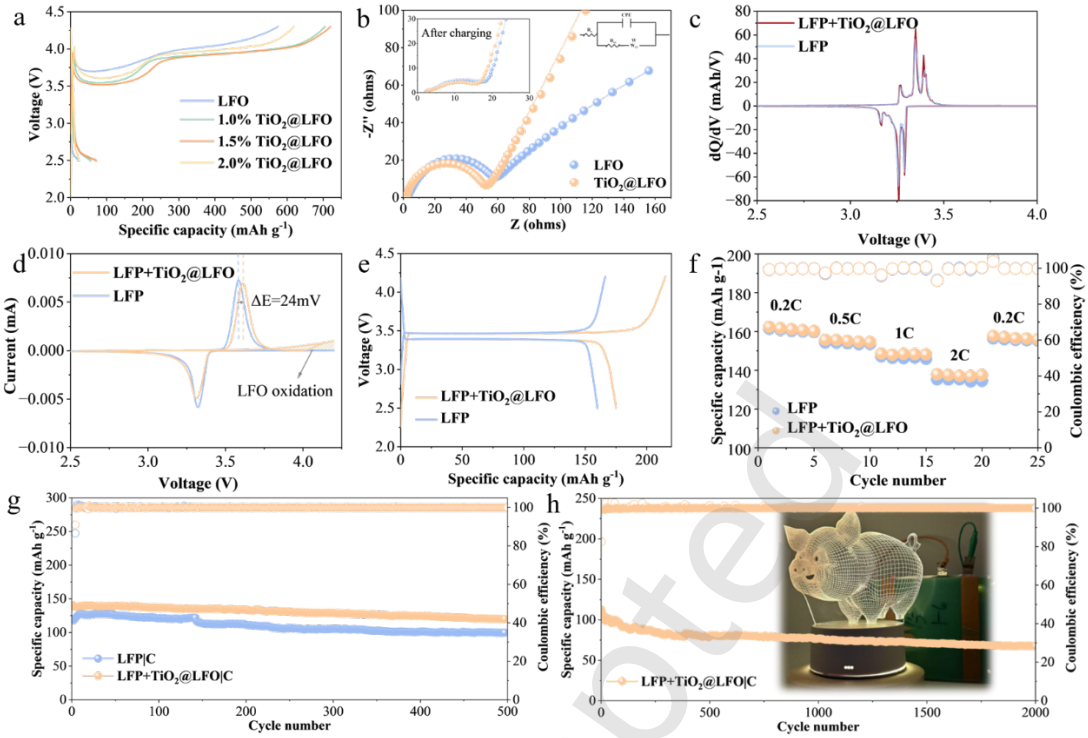

Fig. 5. a Initial charge–discharge curves of different samples; b EIS spectra of LFO|Li and 1.5% TiO_2@LFO|Li half-cells before and after the first charge (the inset shows a magnified view of the EIS after the first charge); c Differential capacity (dQ/dV) curves of full cells during the initial cycle; d CV curves of the initial cycle; e Initial charge–discharge voltage profiles at 0.1C; f Rate performance at different current densities; g Cycling performance at 1C within 2.5–4.2 V; h Cycling performance of the pouch full cell at 1C within 2.5–3.65 V, with the inset showing a photograph of the pouch cell lighting up an LED lamp.

4. Conclusions

In this work, the cycling stability of LFP batteries for energy storage applications is enhanced through the development of a TiO_2-coated LFO cathode prelithiation additive via a combined strategy of high-temperature solid-state synthesis and liquid-phase hydrolysis. Structural characterization reveals that the approximately 1.5% TiO_2 nanocoating achieves uniform coverage over the LFO particle surface without altering the intrinsic anti-fluorite crystal structure of the host material. This surface modification has been shown to effectively mitigate the detrimental reactions of LFO with H_2O and CO_2 upon ambient exposure, enabling the coated sample to retain structural integrity even after 2 h of air exposure while significantly suppressing the formation of alkaline

surface by-products. Consequently, the gelation issue commonly encountered during cathode slurry preparation is markedly alleviated, thereby substantially improving the processing compatibility of the material. Electrochemical evaluations demonstrate that upon incorporation of the TiO_2@LFO compensator into LFP|graphite full cells, an additional charging plateau emerges within the 3.5–4.0 V region, corresponding to the irreversible delithiation of the compensator during the initial charge. This process provides supplementary active lithium to the system, thereby effectively compensating for the lithium inventory consumed by SEI formation on the graphite anode. This, in turn, enhances the initial discharge specific capacity. The results of long-term cycling tests in coin-type full cells indicate that the TiO_2@LFO-containing cells maintain stable capacity output after 500 cycles at 1C, attesting to the favorable cycling compatibility of this compensator in coin-cell configurations. To further evaluate its practical applicability in architectures more representative of commercial battery manufacturing, LFP|graphite pouch cells were assembled and subjected to extended cycling tests. The results show that the pouch cell employing the LFP+TiO_2@LFO cathode delivers an initial discharge specific capacity of 112 mAh g^{-1} and retains 60% of its initial capacity after 2,000 cycles at 1C, with the post-cycled cell still capable of powering an LED lamp. These findings collectively confirm that TiO_2@LFO retains effective lithium compensation capability, cycling adaptability, and reliable energy output in pouch-cell systems. Overall, the surface TiO_2 coating strategy, through precise modulation of the surface chemical environment and interfacial reaction behavior, simultaneously enhances the air stability of LFO while preserving its lithium compensation efficiency, processing compatibility, and cycling robustness in pouch cells. This work provides a viable modification pathway for the development of highly air-stable LFO-based lithium compensators towards practical energy storage applications.

Author contribution statement

Ruijin He and Bo Zhu contributed equally to this work. They jointly conceived the research idea, designed the methodology, and wrote the original draft. Ming Ma,

Minying Wu, and Qiang Fu conducted the experimental investigations, performed data curation, and carried out formal analysis. Zhenyu Jiang, Zhengrong Liu and Qing Li supervised the project, administered the research activities, secured funding, and reviewed and edited the manuscript. All authors have read and approved the final version of the manuscript.

Data availability

The data that support the findings of this study are available from the corresponding author upon reasonable request.

Declaration of competing interest

Ruijin He, Ming Ma, Minying Wu, Qiang Fu, and Zhengrong Liu are employees of Guangdong Power Grid Co., Ltd. The other contributing authors report no conflicts of interest in this work.

Funding

This work was supported by the Science and Technology Project of China Southern Power Grid Company Limited (Grant No. GDKJXM20241276(036100KC24110072)).

Use of AI statement

None.

Electronic Supplementary Material: Supplementary material is available in the online version of this article at https://doi.org/10.26599/EMD.2026.9370111

References

[1] L. Gu, M. Lei, P. Dong, Advanced design strategies for cathode materials of nonaqueous aluminum-ion batteries, Energy Mater. Devices. (2026). https://doi.org/10.26599/EMD.2026.9370090.

[2] Y. Yang, Y. Jin, L. Song, M.-D. Zhang, Efficient Regeneration of Used Lithium Iron Phosphate Cathode Materials Using Dispersants, Energy Technol.

14 (2026) e202502116. https://doi.org/10.1002/ente.202502116.

[3] L. Rathinasamy, B. Natesan, Electrochemical benefits of conductive polymers as a cathode material in LFP battery technology, J. Solid State Electrochem. 28 (2024) 3027–3050. https://doi.org/10.1007/s10008-024-05858-x.

[4] Y. Xu, Z. Tang, X. Zhang, Y. Qian, Q. Wang, Comprehensive Comparison of Different Cooling Methods and Immersion Cooling Liquids for Lithium-ion Batteries [in Chinese], Guangdong Electr. Power. 37 (2024) 45–55. https://kns.cnki.net/kcms2/article/abstract?v=VKKkywmE6pCSlvRdqBuk17FZA7uyVk1L9-5r6x-NhdX9q5E0cqS7Pb75BGuL9ba0YltcxCvS-bx4sRy-jVbPny1IZisldtm5WJzexpOvqmV0fA3iNtvwKYCIDcRf7cpFyhGfnvPLnoxtrH9fds_dDjnCbKxAAcFrG_9I7U0XCvk=&uniplatform=NZKPT&language=CHS.

[5] Y. Gao, W. Chen, J.-S. Park, H. Xu, T. Dai, X. Huang, J. Li, Thick electrodes for electrochemical relithiation to regenerate spent battery powder, Energy Storage Mater. 78 (2025) 104269. https://doi.org/10.1016/j.ensm.2025.104269.

[6] K. Zhang, C. Chen, L. Er, W. Shen, R. Xiong, Robust state-of-charge estimation for $LiFePO_4$ Lithium-ion batteries with pronounced voltage plateau regions, Appl. Energy. 401 (2025) 126755. https://doi.org/10.1016/j.apenergy.2025.126755.

[7] W. Peng, C. Yang, X. Zhong, B. Zhang, State of Charge Estimation for Lithium-ion Batteries Based on Convolutional Past Decomposable Mixing-LSTM Network [in Chinese], Guangdong Electr. Power. 39 (2026) 31–40. https://kns.cnki.net/kcms2/article/abstract?v=VKKkywmE6pDLA2M7uDgG9Y8bJEwT0zN8-lMDhHSCA6HcH_7QZSbBPaMxy-G69vd5V5iQeDcbEw3o3fIO0qS9sOow4UE1mJ6GDeVKAO-kN_fvUSHpdHAtuaia5zOgny3tDuTfiaCM4fCcn1FScaOC6wV8Ku2tN3P86b5L_EzZdGI=&uniplatform=NZKPT&language=CHS.

[8] A.S. Wijareni, F.E. Yunita, Z.T. Ichlas, A. Sumboja, M.Z. Mubarok, Advanced review on $FePO_4$ synthesis process from various Fe sources for $LiFePO_4$ battery cathode precursor material, Ionics (Kiel). 31 (2025) 12545–12573.

https://doi.org/10.1007/s11581-025-06774-4.

[9] Y. Zhang, H. Shen, Y. Li, Y. Hu, Y. Li, Prelithiation strategies for enhancing the performance of lithium-ion batteries, RSC Adv. 15 (2025) 1249–1274. https://doi.org/10.1039/d4ra08234f.

[10] K. Wang, C. Hu, C. Huang, C. Song, W. Xu, S. Huang, Z. Chen, Z. Yang, W. Zhang, Robust Surface-Engineered Li5FeO4 with Enhanced Air Tolerance and Powerful Prelithiation Capability for Lithium-Ion Battery Cathodes, Ind. Eng. Chem. Res. 64 (2025) 20658–20670. https://doi.org/10.1021/acs.iecr.5c02536.

[11] E. Lei, H. Gong, J. Zhang, W. Luo, K. Ma, L. Jin, Z. Chen, Impact of Lithium Plating on the Electrothermal Stability in Battery Systems [in Chinese], Guangdong Electr. Power. 37 (2024) 54–62. https://kns.cnki.net/kcms2/article/abstract?v=VKKkywmE6pBKHGYH1lLJG1P0rjcItXbifdX65Wp5HrldgaxS6DMxrGSgOn7VBDJ97sH1HmB9k_wQtWyJAW8_OqimXjFlwgJHd6YR1aiWmpmybF91LaCXOO2sqd46EDZbLjbLHtfqz_Mpm_uWEIwmehLUajDs2fDtSJdUWeHAxR8=&uniplatform=NZKPT&language=CHS.

[12] J. Wen, B. Qiu, Y. Guan, R. Zhao, G. Xiao, C. He, P. Zhang, Y.-B. He, H. Mi, Defect-Driven Ionic Trap Construction and Interface Modulation for Rapid Li+ Kinetics in Composite Solid Electrolytes, Adv. Mater. 38 (2026) e19541. https://doi.org/10.1002/adma.202519541.

[13] B. Qiu, J. Wen, F. Xu, R. Zhao, C. He, P. Zhang, Z. Lin, H. Mi, Unveiling the Dilution-Shielding Effect as a Universal Strategy for Interfacial Regulation in Composite Polymer Electrolytes, Angew. Chemie Int. Ed. 65 (2026) e8139928. https://doi.org/10.1002/anie.8139928.

[14] A. Li, D. Liu, G. Qin, Z. Jia, S. Sun, H. Wu, J. Chen, Modification of lithium-rich manganese-based cathode materials by continuous coating formed by surface treatment of sodium dodecyl sulfate to improve electrochemical performance, Colloids Surfaces A Physicochem. Eng. Asp. 687 (2024) 133515. https://doi.org/10.1016/j.colsurfa.2024.133515.

[15] W.M. Dose, C. Villa, X. Hu, A.R. Dunlop, M.J. Piernas-Muñoz, V.A. Maroni,

S.E. Trask, I. Bloom, V. Dravid, C.S. Johnson, Beneficial Effect of Li5FeO4 Lithium Source for Li-Ion Batteries with a Layered NMC Cathode and Si Anode, J. Electrochem. Soc. 167 (2020) 160543. https://doi.org/10.1149/1945-7111/abd1ef.

[16] H.A. Lara-García, P. Sanchez-Camacho, Y. Duan, J. Ortiz-Landeros, H. Pfeiffer, Analysis of the CO2 Chemisorption in Li5FeO4, a New High Temperature CO2 Captor Material. Effect of the CO2 and O2 Partial Pressures, J. Phys. Chem. C. 121 (2017) 3455–3462. https://doi.org/10.1021/acs.jpcc.6b12431.

[17] M.V. Blanco, K. Kohopää, I. Snigireva, F. Cova, Low temperature solid state synthesis of Li5FeO4 and CO2 capture mechanism via real time in situ synchrotron X-ray diffraction, Chem. Eng. J. 354 (2018) 370–377. https://doi.org/10.1016/j.cej.2018.08.017.

[18] N. Wang, C. Hernández-Fontes, W.E. Vallejo Narváez, S. Fomine, H. Pfeiffer, Unraveling the Textile Pollution Problem with Li5FeO4 as a Bifunctional Material for Hydrogen Production and COx Capture: From Glucose to Cotton Pyrolysis, ACS Sustain. Chem. Eng. 12 (2024) 13163–13175. https://doi.org/10.1021/acssuschemeng.4c03359.

[19] Y. Cheng, Z. Jiang, P. Li, H. Guo, W. Zhao, B. Yan, D. Chen, CO2 capture and regeneration characteristics of pentalithium ferrite (Li5FeO4), Mater. Today Commun. 38 (2024) 108370. https://doi.org/10.1016/j.mtcomm.2024.108370.

[20] J. Yan, L. Wang, Y. Dou, N. Zhang, C. Zhao, S. Wang, Y. Shi, X. Zhu, H. Zhang, L. Mu, Q. Tang, Anchoring Li3PO4 on Li5FeO4 Surface as a Prelithiation Additive for Lithium-Ion Batteries, Langmuir. 41 (2025) 26605–26613. https://doi.org/10.1021/acs.langmuir.5c02365.

[21] C. Liu, H. Zhang, W. Zhou, X. Tian, T. Zhang, S. Niu, J. Li, M. Cao, Q. Wang, F. Lv, T. Peng, L. Tao, X. Rang, Z. Chen, X. Su, Air-stable Li5FeO4 additive enabled by carbon coating for energy-dense lithium-ion batteries, Nat. Commun. 16 (2025) 7694. https://doi.org/10.1038/s41467-025-62418-1.

[22] B. Zhu, N. Wen, J. Wang, Q. Wang, J. Zheng, Z. Zhang, Defect engineering of

air-stable Li5FeO4 towards an ultra-high capacity cathode prelithiation additive, Chem. Sci. 15 (2024) 12879–12888. https://doi.org/10.1039/d4sc03052d.

[23] B. Zhu, W. Zhang, Q. Wang, Y. Lai, J. Zheng, N. Wen, Z. Zhang, Understanding the Air-Exposure Degradation Chemistry of the Sacrificial Cathode Additive Li5FeO4 for Li-Ion Batteries, Adv. Funct. Mater. 34 (2024) 2315010. https://doi.org/10.1002/adfm.202315010.

[24] L. Niu, M. Wu, Y. Zhang, C. Gao, X. Li, H. Ding, N. He, P. Wang, J. Zhang, J. Yan, N. Zhang, D. Zhao, X. Cui, S. Li, Surface phosphorylated Li5FeO4 prelithiation additive synergistically improves the air-stability and lithium-ion conductivity, Chem. Eng. J. 498 (2024) 155242. https://doi.org/10.1016/j.cej.2024.155242.

[25] Z.-R. Yan, D.-F. Tang, B.-H. Wang, X.-J. Huang, X. Zou, S.-C. Fan, Y. Wu, T. Shu, Q.-L. Wei, Hybrid pseudocapacitance/co-intercalation mechanisms of TiO2/graphite anodes for rapid sodium-ion storage, Rare Met. 43 (2024) 5427–5434. https://doi.org/10.1007/s12598-024-02848-w.

[26] X. Song, W. Huang, R. Ge, H. Wang, J. Xing, Electrospun Nanofibers Constituted of a Polyimide Core Decorated with Polyhedral Oligomeric Silsesquioxanes and a TiO2 Shell as Separators for Lithium-Ion Batteries, ACS Appl. Nano Mater. 7 (2024) 21565–21577. https://doi.org/10.1021/acsanm.4c03481.

[27] P. Wang, H. Norimatsu, X. Chen, K. Matsuhira, J. Liu, E. Lin, M. Zhang, S. Fang, Y. Sakurai, T. Matsubara, T. Hihara, L. Pan, W. Zhang, Z. Sun, X. Li, S.-Z. Kure-Chu, Low-cost, scalable-fabrication, binder-free TiO2/TiO2–TiN/MoS2 nanostructured composite anode for high-areal-capacity lithium-ion batteries, J. Energy Storage. 142 (2026) 119540. https://doi.org/10.1016/j.est.2025.119540.

[28] Z. Ahaliabadeh, V. Miikkulainen, M. Mäntymäki, M. Colalongo, S. Mousavihashemi, L. Yao, H. Jiang, J. Lahtinen, T. Kankaanpää, T. Kallio, Stabilized Nickel-Rich-Layered Oxide Electrodes for High-Performance

Lithium-Ion Batteries, ENERGY Environ. Mater. 7 (2024) e12741. https://doi.org/10.1002/eem2.12741.

[29] W.-M. Chen, H.-Y. Hsieh, D.-Z. Wu, H.-Y. Tang, K.-S. Chang-Liao, P.-W. Chi, P.M. Wu, M.-K. Wu, Advanced TiO2/Al2O3 Bilayer ALD Coatings for Improved Lithium-Rich Layered Oxide Electrodes, ACS Appl. Mater. Interfaces. 16 (2024) 13029–13040. https://doi.org/10.1021/acsami.3c16948.

[30] X. Cai, N. Zhang, J. Wang, X. Zhou, F. Xu, H. Ding, P. Wang, L. Song, J. Huang, X. Fu, X. Cui, C. Yang, S. Li, Understanding mechanism of voltage decay and temperature sensitivity of Li-rich manganese-based cathode materials, Mater. Des. 225 (2023) 111548. https://doi.org/10.1016/j.matdes.2022.111548.

[31] B. Luo, J. Wu, M. Zhang, Z. Zhang, X. Zhang, Z. Fang, Z. Xu, M. Wu, Surface modification of garnet fillers with a polymeric sacrificial agent enables compatible interfaces of composite solid-state electrolytes, Chem. Sci. 14 (2023) 13067–13079. https://doi.org/10.1039/d3sc04710e.

[32] A. Laurita, L. Zhu, P.-E. Cabelguen, J. Auvergniot, D. Guyomard, P. Moreau, N. Dupré, Residual Li2O degrades PVdF during the preparation of NMC811 slurries for Li-ion batteries, Chem. Commun. 59 (2023) 4951–4953. https://doi.org/10.1039/d3cc00471f.